*Key Engineering Materials*
*ISSN: 1662-9795, Vol. 1050, pp 227-234*
*doi:10.4028/p-E8wywR*

*Submitted: 2026-01-21*
*Revised: 2026-03-02*
*Accepted: 2026-03-02*
*Online: 2026-04-16*

# Modelling Deformation Mechanisms Decomposition, Separation and Compaction in Mechanical Joining Processes of Fiber Reinforced Thermoplastics on Meso Scale

Benjamin Gröger[a,1*], Johannes Gerritzen[b,1], Andreas Hornig[c,1,2,3] and Maik Gude[d,1]

[1]Institute for Lightweight Engineering and Polymer Technology (ILK), TUD Dresden University of Technology, Holbeinstrasse 3, 01307 Dresden (Germany)

[2]Department of Engineering Science, Solid Mechanics and Materials Engineering, University of Oxford, Oxford, OX1 3PJ, United Kingdom

[3]Center for Scalable Data Analytics and Artificial Intelligence Dresden/Leipzig (ScaDS.AI), TUD Dresden University of Technology, Strehlener Straße 12-14, Dresden, 01069, Germany

[a]benjamin.groeger@tu-dresden.de, [b]johannes.gerritzen@tu-dresden.de, [c]andreas.hornig@tu-dresden.de, [d]maik.gude@tu-dresden.de (*corresponding author)

**Keywords:** Composite-Metal Joining, Simulation, Fluid-Structure-Interaction, Finite Element Method (FEM)

**Abstract.** The mechanical joining of continuous fiber-reinforced thermoplastics (cFRTP) and metal sheets represents a promising approach for manufacturing hybrid lightweight structures. To reduce the time and cost associated with extensive experimental investigations, numerical modeling strategies are increasingly applied. In this numerical study, a further step in the modelling strategy for the direct pin-pressing (DPP) process of cFRTP and metal sheets is presented. The study focuses on modeling and simulating the occurring deformation mechanisms of decomposition, compaction, and separation of individual rovings on the mesoscale to analyze the resulting material structure. For this purpose, two simplified models were derived. The textile architecture is represented based on micrographs of cross-sections and discretized using the finite element method. The deformation of individual rovings during joining leads to a deformation of their initial elliptical cross section. To capture this level of resolution, both a cohesive zone and a pure contact approach are applied within the rovings. The highly viscous thermoplastic melt is modeled as a fluid employing the Arbitrary Lagrange–Eulerian (ALE) method. Matrix and roving meshes are coupled to account for fluid–structure interaction (FSI) during process. The study shows that coupling of matrix and rovings is necessary to obtain more accurate predictions of the deformation behaviour. Furthermore, the cohesive zone approach is better suited to simulate the emerging deformation mechanisms.

## Introduction

Continuous fiber reinforced plastics (cFRTP) are widely used in industrial applications due to their outstanding specific strength and stiffness. In contrast to thermosetting matrix systems, cFRTP enable shorter cycle times and easier forming during processing, primarily due to their temperature-dependent forming behavior, especially above the melting temperature. Additionally, the handling of the semi-finished products so called organo-sheets, is easier and faster at room temperature. As a result, the use of hybrid structures combining metals and cFRTP has increased, which leads to challenging tasks for joining dissimilar materials [1] and subsequently to develop methodologies to reliably join metals and cFRTP [1,2]. Mechanical joining technologies generate a form closure by plastic deformation with the occurrence of fiber failure and delamination (e.g. [3]). Alternatively, when the thermoplastic matrix is above its melting temperature, fiber rearrangement processes can occur (cf. [4,5]). The rearrangement process is driven by process route (e.g. heating strategy) [6], tool design and concept [7,8], material system [9] as well as process parameters (e.g. tool velocity, process temperature). To date, investigations have been primarily based on experimental approaches due to the lack of suitable numerical methods for simulating such local forming processes. However,

experimental setups require fundamental decisions regarding the tool concept and process configuration, which limit parameter variation and constrain the development process.

During the joining process of metal sheets and organo-sheets above melting temperature fiber deformation and rearrangement [10] as well as matrix flow process [11] due to the motion and deformation of the joining partner and tools occur. Numerical simulations of the joining process are capable of predicting the resulting material structure of the cFRTP, including changes in fiber orientation and the formation of matrix-rich zones. Accurate prediction of the resulting material structure requires a scale-specific modeling approach, in which fibers and matrix are modeled separately [12,13], commonly referred to as direct numerical simulation. However, modeling individual fibers, the matrix, and the associated fluid-structure interaction (FSI) on the microscale requires very high computational efforts. Therefore, modeling approaches on the sub-mesoscale based on fiber bundles [14–16] or meso scale [17] for cFRTP are appropriate. These approaches enable the prediction of fiber rearrangement and deformation mechanisms as well as matrix flow processes. When using fabrics, deformation mechanisms of the rovings, such as decomposition, compaction, and separation, can be observed (Fig. 1).

The numerical method for these flow process simulations are often based on Arbitrary-Lagrange-Eulerian (ALE) method [18], which allows to simulate a flow of fluid or ductile materials [12,17,19]. Within the fluid zone, solid structures (e.g. fibers, fiber bundles, tools) can be embedded and coupled. The coupling can be achieved either via velocity-field-based force transfer [12,20] or penalty-based or constraint-based coupling schemes [21].

In order to develop a modelling strategy for mechanical joining technologies, the novel DPP developed in [4] is chosen as a representative example. Based on the experimental investigation of this DPP by Popp et al. [6,7,9], a first numerical simulation approach on the sub-mesoscale using fiber bundles was proposed by Gröger et al. [19].

In the present work, the modeling strategy is extended to the mesoscale by explicitly accounting for the textile architecture and the roving geometry in order to predict the deformation mechanisms of decomposition, compaction, and separation (Fig. 1). Modeling the individual yarns with deformable cross-sections results in severe numerical instabilities due to the large deformation degrees of freedom. Therefore, a dedicated numerical study is conducted to systematically investigate and model these dominant mechanisms.

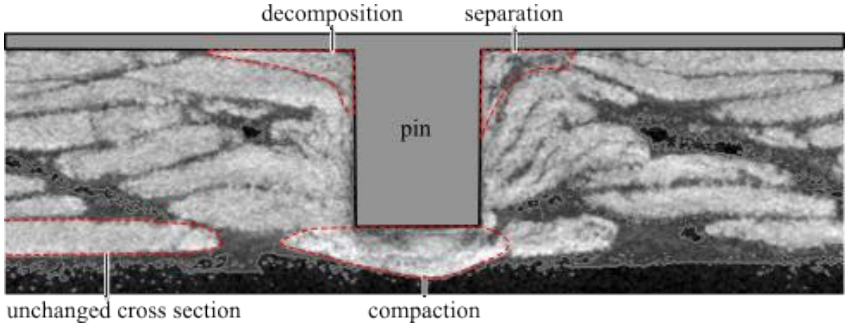


**Fig. 1.** Computed tomography scan of the resultant material structure after DPP with the occurring mechanism of compaction, decomposition and separation of the rovings

## Materials and Methods

The presented paper investigates a non-crimp fabric (NCF) made of glass fibers previously studied in [19], combined with a polypropylene (PP) matrix material (Borealis BJ100-HP), using DPP joining process improved by Popp et al. [7]. The principle of the joining process is illustrated in Fig. 2.

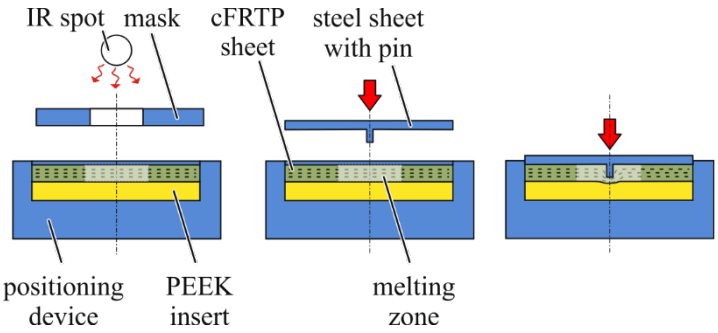


**Fig. 2.** Illustration of the DPP process in three steps according to Popp et al. [7], adapted from [19]

**Joining process.** During the joining process, the organo-sheet is placed in a positioning device and elastically supported by a PEEK insert. A mask with a circular opening is positioned above the sheet, and an infrared (IR) spot selectively heats the organo-sheet to approximately 180 °C at the bottom and 300 °C at the top. This creates a zone of molten matrix in the area underneath the mask opening, while the surrounding material remains solid to suppress undesired fiber rearrangement. After heating, a steel sheet with a pin is pressed into the cFRTP at a defined velocity with $v$ = 100 mm/s. Subsequently, a constant compression force is maintained during a relaxation phase, completing the joining process as the organo-sheet cools below its melting temperature.

**Material modelling.** The matrix is modeled as a compressible shear-thinning fluid (*MAT_ALE_VISCOUS) with material parameters of the PP at 200 °C from [19]. The shear-rate-dependent viscosity is implemented via a tabulated function following a regularized CROSS model [22]. The corresponding parameters $\eta_\infty$ as infinite-shear viscosity, $\eta_0$ as zero-shear viscosity, and the both CROSS parameters $\lambda$ and $n$ are listed in Table 1 and were experimental determined in [19]. In addition, the dependency of density on hydrostatic pressure, commonly referred to as an equation of state (EOS), is described by the Murnaghan model, given as

$$\Delta p = k_0 \left[ \left( \frac{\rho}{\rho_0} \right)^{\gamma} - 1 \right]. \tag{1}$$

Here, $\rho_0$ denotes the initial density at atmospheric pressure and 200 °C, while $k_0$ and $\gamma$ are material coefficients of the EOS model. The EOS parameters are fitted by experimental trails with the high pressure capillarity rheometer GÖTTFERT RHEOGRAPH 75 [19]. Due to the use of the ALE-method for the PP melt flow process an EOS is mandatory.

**Table 1.** Coefficients of the Cross model describing the shear-rate-dependent viscosity and parameters of the Murnaghan EOS for the PP matrix at 200 °C, taken from [19]

| Cross model | | | | EOS | | |
|---|---|---|---|---|---|---|
| $\eta\infty$ [Pa s] | $\eta0$ [Pa s] | $\lambda$ [s] | n | $\rho0$ [to/mm$^3$] | $k0$ [MPa] | $\gamma$ |
| 2.68 | 328.22 | 0.040 | 0.59 | 7.42e-10 | 103.1 | 6.519 |

As concluded by Gröger et al., the textile architecture must be represented in detail for the mesoscale modeling approach [19]. To allow for an efficient assessment of the rovings' behavior, they are modeled as solid, with orthotropic plasticity as surrogate for the material flow. For this, a Hill type yield surface is chosen (*MAT_122_3R_3D). Given the challenge of determining material parameters above the melting temperature experimentally, parameters from a preliminary numerical study presented in [23] are adopted and extended. They identified a maximum flow stress of $\sigma max$ = 0.308 MPa, both for shear as well as transverse loading. Hence, $\sigma max$ is taken as surrogate yield strength under all uniaxial loadings apart from that in the fiber direction. Since high temperature compression tests revealed negligible flow in this direction [24], an arbitrary high strength of 1 GPa is assumed, effectively limiting flow in this direction, as shown in [25]. Since the analyses in [23] did not exhibit an increase of deformation resistance with increasing flow, no hardening was

implemented. The resulting surrogate material parameters are summarized in Table 2. With the direction-dependent elastic constants and HILL yield potential parameters *F*, *G*, *H*, *L*, *M*, and *N*.

**Table 2.** Orthotropic elastic and plastic material properties of the homogenized GF/PP roving

*Elastic constants*

| Property | *E*1 [MPa] | *E*2 [MPa] | *E*3 [MPa] | *G*12 [MPa] | *G*13 [MPa] | *G*23 [MPa] | *v*12 [-] | *v*13 [-] | *v*23 [-] |
|---|---|---|---|---|---|---|---|---|---|
| Value | 44,380 | 10.8 | 10.8 | 3.91 | 3.91 | 3.84 | 0.49 | 0.49 | 0.49 |

*Plastic HILL yield potential parameters*

| Property | *F* | *G* | *H* | *L* | *M* | *N* | $\sigma_{max}$ |
|---|---|---|---|---|---|---|---|
| Value | 0.999 | 4.7e-8 | 4.7e-8 | 0.5 | 0.5 | 0.5 | 0.308 |

The geometric dimensions of the NCF are determined by computed tomography (CT) scans and are illustrated in Fig. 3. Gröger et al. [19] measured the characteristic dimensions of the NCF and assumed a total layer thickness of 0.25 mm in order to model eight layers, resulting in an overall organo-sheet thickness of 2 mm. The height of an individual roving was measured to be 0.32 mm.

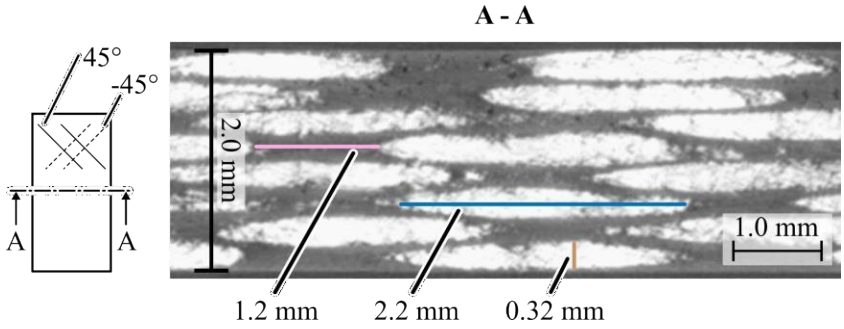


**Fig. 3.** CT scan of the pre-consolidated organo sheet made of non-crimped glass fiber fabric (white) and PP (gray) with the characteristic dimensions (average) measured in [19]

## Numerical Setup

The numerical setup follows the results of Gröger et al. [19], using LS-DYNA R16.1.0 mpp with double precision. The process model includes a conical pin with a root diameter $d_{Pin}$ of 1.25 mm, a tip diameter $D_{Pin}$ of 1.50 mm, and a height $h_{Pin}$ of 1.80 mm (Fig.4 top). To reduce the computational effort, the setup is simplified to a single-roving (1R) and a two-roving (2R) model. Each roving with a total length of 0.8 mm is discretized using four finite elements along the fiber direction and two elements in the thickness direction (Fig. 4, bottom). To enable the modeling of roving decomposition and separation, two different approaches are investigated. In the first approach, cohesive zone (CZ) elements are implemented between the mid-section of the roving and two additional planes along the thickness direction (Fig. 4 top right, purple elements). The bilinear material behavior of the CZ elements is defined using the parameters reported in [23]. The parameters are based on representative volume cells on micro scale with PP melt and glass fibres under shear and normal stress. In the second approach, the roving elements are separated geometrically and interact solely via a frictionless contact definition, without the use of CZ elements. Both the CZ-based and the separation-based (Sep) models employ a coupling between the fluid matrix and the solid structures using a penalty based coupling method (*CONSTRAINED_LAGRANGE_IN_SOLID) [21]. The rovings are fully embedded in the matrix material, which is allowed to flow through the elements of the ALE domain. The vertical boundaries of the ALE domain are constrained to prevent material flow in the normal direction. In addition, the lateral motion of the rovings is restricted by rigid walls on both sides transverse to the fiber direction, while the roving ends are only permitted to move within the cross-sectional plane. To avoid excessive element distortion at the roving ends, the rotationally symmetric pin geometry is

simplified to a cuboid extending along the full roving length. The height and width of the cuboid correspond to the pin height $h_{Pin}$ and the tip diameter $D_{Pin}$. This cuboid is driven downward in a displacement-controlled manner with the same velocity $v$ as the original pin. The rovings are positioned between the tool above and a rigid block below, at which the reaction forces $F_z$ are recorded for comparison. While the 1R model primarily focuses on roving compaction beneath the pin, the 2R model emphasizes the interaction between neighbouring rovings, particularly with respect to decomposition and separation mechanisms.

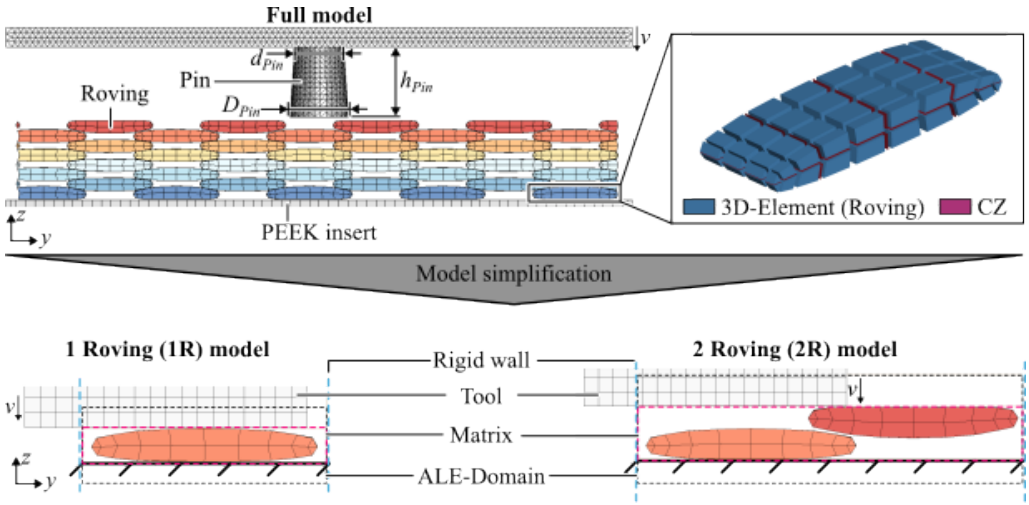


**Fig. 4.** Simplified models of the DPP with increasing complexity from 1R to 2R model

## Results

The reaction force $Fz$ is shown in Fig. 5. For the 1R model, both investigated approaches exhibit only a slight increase in reaction force with increasing compaction defined by the tool displacement $\Delta z$ and the initial tool-PEEK-insert distance $z_0$ via compaction $= \frac{z_0 - \Delta z}{z_0}$.

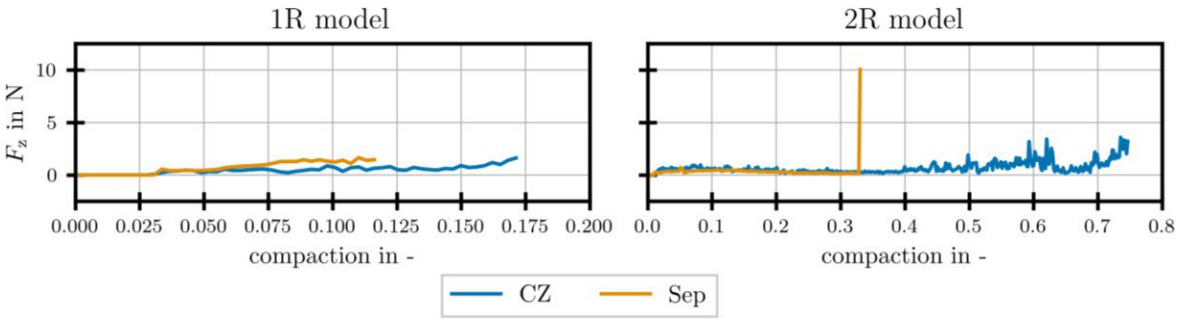


**Fig. 5.** Reaction force $Fz$ at the rigid block for each model and the two modelling approaches of CZ-based and separation-based model

However, the CZ-based approach allows a higher degree of compaction before numerical instability occurs. A similar trend is observed for the 2R model. For the 2R model, both approaches initially show an increase in reaction force due to the first contact between the tool and the rovings. The subsequent decrease in force at a compaction $\varepsilon$ of approximately 0.1 can be attributed to the lateral displacement of the upper roving out of the cavity. At a compaction level of around 0.32, the separation-based model becomes numerically unstable and collapses, accompanied by an abrupt increase in reaction force. In contrast, the CZ-based model remains stable up to a compaction of approximately 0.75 and exhibits an increasing but unsteady force response, which is mainly caused by the continued contact with the tool and the progressive compaction of the lower roving.

For further evaluation of the CZ-based and separation-based models, the resulting deformation of the rovings and the matrix is illustrated in Fig. 6. In the 1R-CZ model, the roving retains a continuous

structure despite the higher degree of compaction. In contrast, the separation-based model exhibits a lower level of compaction, and the roving remains separated even though the matrix restricts the motion via fluid-structure coupling. The matrix flow appears physically plausible, as the molten material is displaced outward from the cavity.

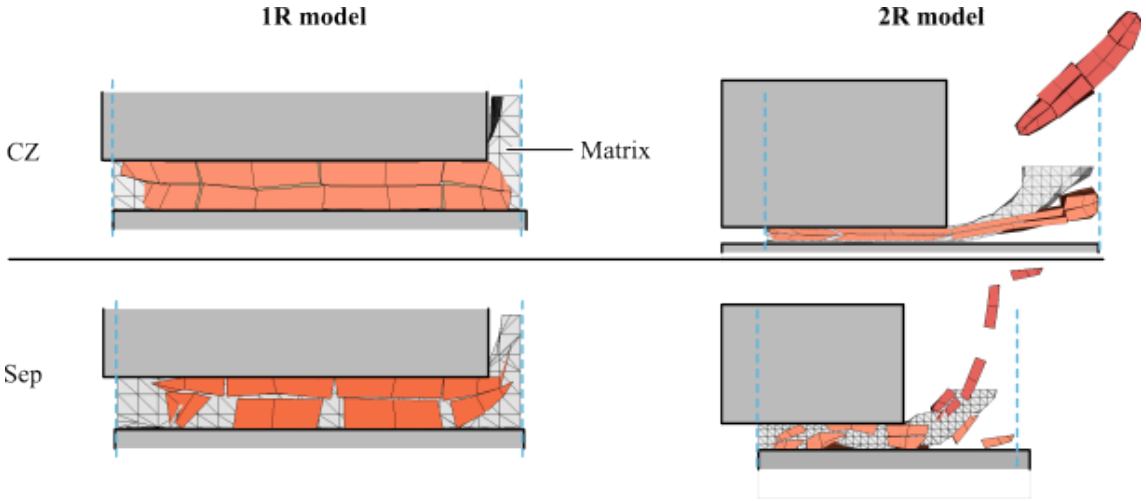


**Fig. 6.** Deformation of the rovings and matrix flow during compaction for each model

For the 2R models, increased motion and deformation of the roving elements are observed. In the CZ-based approach, the roving located directly beneath the tool is strongly compressed while remaining continuous. The adjacent roving moves laterally away from the tool, which indicates that the coupling forces between the matrix and the roving may be underestimated. In the separation-based model, both rovings exhibit pronounced separation and reduced compaction. The outward motion of roving elements from the cavity is considered responsible for the abrupt increase in reaction force and the subsequent numerical collapse. This behavior becomes even more pronounced when no coupling between the roving elements and the matrix is considered, confirming the importance of fluid-structure interaction for numerical stability and realistic material deformation. Furthermore, the dynamic effects caused by the high tool velocity during joining induce rigid body motion once interactions between rovings occur. This has to be considered in full-scale simulations, as it may result in excessive and nonphysical element distortion of the roving elements. Therefore, this qualitative numerical study provides essential insight for future full-process simulations and further model development.

## Summary

The presented results indicate that the CZ-based approach is more suitable for simulating the resulting material structure of the DPP process, particularly with respect to roving compaction and decomposition when considering fluid-structure interaction. Moreover, the CZ-based model exhibits improved numerical stability compared to a purely separation-based approach. The proposed mesoscale modeling strategy represents a computationally efficient compromise between microscale and macroscopic approaches and enables the investigation of local deformation mechanisms in cFRTP joining processes. Nevertheless, further refinement of the roving material model is required to reduce element distortion at free roving edges. Planned squeeze experiments will provide material parameters for thickness compaction and serve as a basis for future model validation. In the long term, the approach offers significant potential for simulation-based process development of hybrid metal-cFRTP joints.

In future work, the material model of the roving needs to be further refined in order to reduce element distortion at the free edges of the rovings. For this purpose, squeeze experiments will be conducted to identify material parameters governing compaction in the thickness direction.

**Acknowledgements**

The authors gratefully acknowledge

- The computing time made available to them on the high-performance computer at the NHR Center of TU Dresden. This center is jointly supported by the Federal Ministry of Research, Technology and Space of Germany and the state governments participating in the NHR (www.nhr-verein.de/unsere-partner).
- The subproject C04 of the Collaborative Research Centre TRR285/2 for CT data and measurements.

**Fundings**

This research was funded by the Deutsche Forschungsgemeinschaft (DFG, German Research Foundation) – TRR 285/2 – 418701707 subproject A03.

**References**

[1] Lambiase F, Scipioni SI, Lee C-J, Ko D-C, Liu F. A State-of-the-Art Review on Advanced Joining Processes for Metal-Composite and Metal-Polymer Hybrid Structures. Materials (Basel) 2021;14(8).

[2] Galińska A, Galiński C. Mechanical Joining of Fibre Reinforced Polymer Composites to Metals-A Review. Part II: Riveting, Clinching, Non-Adhesive Form-Locked Joints, Pin and Loop Joining. Polymers (Basel) 2020;12(8).

[3] Lambiase F, Paoletti A. Friction-assisted clinching of Aluminum and CFRP sheets. Journal of Manufacturing Processes 2018;31:812–22.

[4] Kraus M, Frey P, Kleffel T, Drummer D, Merklein M. Mechanical joining without auxiliary element by cold formed pins for multi-material-systems. ESAFORM 2019. p. 50006, 2019.

[5] Brown N, Worrall CM, Ogin SL, Smith PA. Investigation into the mechanical properties of thermoplastic composites containing holes machined by a thermally-assisted piercing (TAP) process. Advanced Manufacturing: Polymer & Composites Science 2015;1(4):199–209.

[6] Popp J, Drummer D. Investigation of different process routes for joining thermoplastic composite/steel joints via the embedding of cold formed metallic pin structures. Journal of Advanced Joining Processes 2024;10(12):100271.

[7] Popp J, Drummer D. Joining of continuous fiber reinforced thermoplastic/steel hybrid parts via undercutting pin structures and infrared heating. Journal of Advanced Joining Processes 2022;5(3):100084.

[8] Römisch D, Popp J, Drummer D, Merklein M. Joining of CFRT-steel hybrid parts via hole-forming and subsequent pin caulking. Prod. Eng. Res. Devel. 2022;16(2-3):339–52.

[9] Popp J, Drummer D. Influence of the Textile Reinforcement on the Joint Formation of Pin-Joined Composite/Metal Parts. Appl Compos Mater 2024;31(3):799–822.

[10] Akkerman R, Haanappel SP, Sachs U. History and future of composites forming analysis. IOP Conf. Ser.: Mater. Sci. Eng. 2018;406:12003.

[11] Barnes JA, Cogswell FN. Transverse flow processes in continuous fibre-reinforced thermoplastic composites. Composites 1989;20(1):38–42.

[12] Meyer N, Schöttl L, Bretz L, Hrymak AN, Kärger L. Direct Bundle Simulation approach for the compression molding process of Sheet Molding Compound. Composites Part A: Applied Science and Manufacturing 2020;132(1):105809.

[13] Gude M, Freund A, Vogel C, Kupfer R. Simulation of a Novel Joining Process for Fiber-Reinforced Thermoplastic Composites and Metallic Components. Mech Compos Mater 2017;52(6):733–40.

[14] Green SD, Long AC, El Said B, Hallett SR. Numerical modelling of 3D woven preform deformations. Composite Structures 2014;108:747–56.

[15] Döbrich O, Gereke T, Cherif C. Modeling the mechanical properties of textile-reinforced composites with a near micro-scale approach. Composite Structures 2016;135(14):1–7.

[16] Gereke T, Döbrich O, Malik SA, Kocaman RT, Aibibu D, Schmidt K et al. Numerical micro-scale modelling of the mechanical loading of woven fabrics equipped with particles. IOP Conf. Ser.: Mater. Sci. Eng. 2018;460:12006.

[17] Gröger B, Hornig A, Hoog A, Gude M. Modelling of thermally supported clinching of fibre-reinforced thermoplastics: Approaches on mesoscale considering large deformations and fibre failure. ESAFORM 2021, 2021.

[18] Donea J, Huerta A, Ponthot J-P, Rodríguez-Ferran A. Arbitrary L agrangian– E ulerian Methods. In: Stein E, editor. Encyclopedia of computational mechanics. Hoboken, NJ: Wiley; 2006, p. 14.

[19] Gröger B, Gerritzen J, Hornig A, Gude M. Developing a numerical modelling strategy for metallic pin pressing processes in fibre reinforced thermoplastics to investigate fibre rearrangement mechanisms during joining. Proceedings of the Institution of Mechanical Engineers, Part L: Journal of Materials: Design and Applications 2024;238(12):2286–98.

[20] Lindström SB, Uesaka T. Simulation of the motion of flexible fibers in viscous fluid flow. Physics of Fluids 2007;19(11):111.

[21] Benson DJ, Okazawa S. Contact in a multi-material Eulerian finite element formulation. Computer Methods in Applied Mechanics and Engineering 2004;193(39-41):4277–98.

[22] Cross MM. Rheology of non-Newtonian fluids: A new flow equation for pseudoplastic systems. Journal of Colloid Science 1965;20(5):417–37.

[23] B. Gröger, J. Gerritzen, M. Gude. Modeling approaches for the decomposition behavior of preconsolidated rovings throughout local deformation processes. SheMet 2025.

[24] Gröger B, Römisch D, Kraus M, Troschitz J, Füßel R, Merklein M et al. Warmforming Flow Pressing Characteristics of Continuous Fibre Reinforced Thermoplastic Composites. Polymers (Basel) 2022;14(22).

[25] Gerritzen J, Gröger B, Zscheyge M, Hornig A, Gude M. 3D viscoelastic plastic model coupled with a continuum damage formulation for fiber reinforced polymers. Materials & Design 2025;260:114969.